学　位　論　文

Studies on molecular imaging in traumatic brain injury with neurobehavioral disability

(高次脳機能障害を呈した外傷性脳損傷における分子イメージングに関する研究)

2018 年 3 月

北海道大学

安彦かがり

学　位　論　文

Studies on Molecular imaging in Traumatic brain injury with neurobehavioral disability

(高次脳機能障害を呈した外傷性脳損傷における分子イメージングに関する研究)

2018 年 3 月

北海道大学

安彦かがり

Contents

List of publications and presentations

Part of the research has been published as listed below:

1. Kagari Abiko, Katsunori Ikoma, Tohru Shiga, Chietsugu Katoh, Kenji Hirata, Yuji Kuge, Kentaro Kobayashi, Nagara Tamaki. I-123 iomazenil single photon emission computed tomography for detecting loss of neuronal integrity in patients with traumatic brain injury. *EJNMMI research* **7**, 28, (2017).
2. Kagari Abiko, Tohru Shiga, Chietsugu Katoh, Kenji Hirata, Yuji Kuge, Kentaro Kobayashi, Satoshi Ikeda, Katsunori Ikoma. Relationship between Intelligence Quotient (IQ) and Cerebral Metabolic Rate of Oxygen in Patients with Neurobehavioral Disability after Traumatic Brain Injury. *Brain injury* (under review)

Part of the research has been presented in the conference as listed below:

1. Kagari Abiko, Tohru Shiga, Katsunori Ikoma. The relationship between IQ and CMRO2 for traumatic brain injury with higher brain dysfunction. 10th International Society of Physical and Rehabilitation Medicine World Congress. May, 2016. Kuala Lumpur, Malaysia

Introduction

In Japan, 27 per 100,000 persons yearly are hospitalized for a traumatic brain injury (TBI) [1], and the severity of injury classified by the Glasgow Coma Scale (GCS) at the time of admission has been as follows: mild 70%, moderate 10%, and severe 20%. The overall outcomes were categorized as good recovery 67.3%, moderate disability 11.3%, and severe disability 5.7%. However, the patients who did not require hospitalization were excluded from that analysis, and the actual number of patients with mild TBIs is higher.

It was reported that approx.15% of TBI patients have persistent neurobehavioral impairments, even among those who suffered a mild head injury [2]. Approximately 20% of overall patients with a TBI may have persistent neurobehavioral impairments including the symptoms described above.

TBI causes brain dysfunction in many patients. Disturbed cognition is the hallmark symptom of TBI[3], because focal injury is likely to occur in the frontotemporal lobe, and diffuse injury causes many forms of damage over a widespread area. In individuals who have incurred a TBI, cognitive disturbance rather than physical disturbance is characteristic.

Many of the forms of cognitive disturbance caused by a TBI cannot be explained only by the site of the brain injury detected by magnetic resonance imaging (MRI).

Neurobehavioral disabilities such as impaired attention, memory disorder, and executive function disorder interfere with TBI patients' education and employment opportunities, causing serious economic losses and a significant decrease in the quality of their daily life. It is thus important to promptly make an accurate diagnosis, understand the clinical conditions, and provide rehabilitation and support to TBI patients on the basis of the diagnosis. Even patients who have suffered a mild head injury may experience after-effects that significantly and adversely affect their daily lives, including fatigue, memory disorder, and poor concentration [4-6].

Cognitive dysfunctions such as aphasia, agnosia, apraxia, are clearly localized in brain function, and easily noticed in hospitalized living. The symptoms of a more advanced cognitive function disorder (e.g., not being able to concentrate on work, not being able to do multiple tasks at the same time) are not clearly localized in brain function and are often not noticed in specialized environments such as hospitals. These symptoms are often observed only after the patient returns to society. Patients with a brain injury who do not show residual focal neurological symptoms such as paralysis and aphasia are often discharged to return home after the acute phase, without confirmation of the need for rehabilitation.

According to a survey conducted in Tokyo (a metropolitan area of approx. 12.8

million residents), 3,010 individuals (23/100,000 individuals) per year suffer from cognitive and behavioral changes as a result of brain damage, and the rate of TBIs in this population is estimated to be about 10% [7]. This is lower than the number of patients suffering from neurobehavioral disability estimated from the epidemiology of TBI. There is a possibility that TBI patients are missed without being diagnosed.

After having returned to society, such patients notice attention disorder and concentration, and consult a hospital. However, because the lesions often become unclear in the chronic phase (Figure 1), they may not be evaluated correctly and may not receive appropriate medical care.

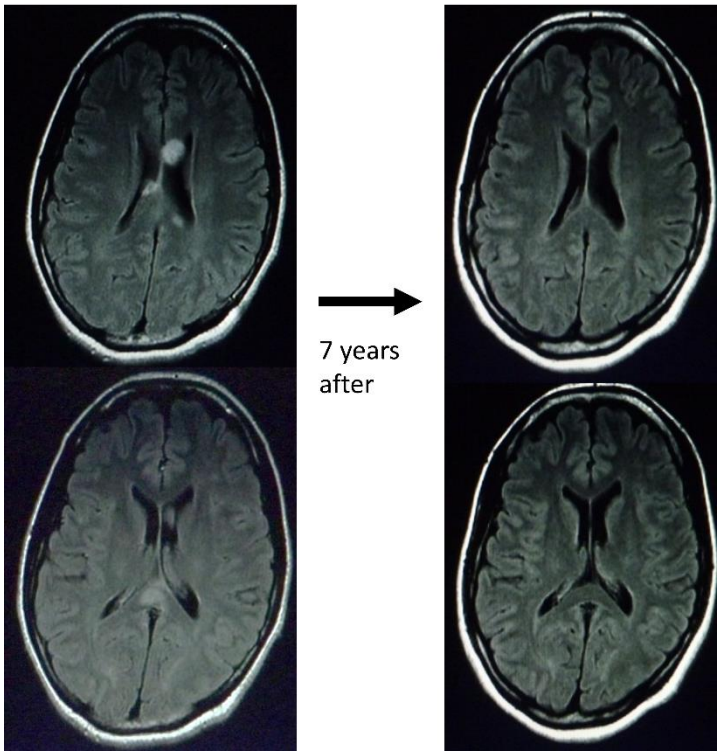

Figure 1. A case of DAI.
The high intensity area of MRI FLAIR, which was found in the corpus callosum in the acute phase, disappeared in the chronic phase.

Neurobehavioral disability caused by TBI has the following characteristics, microscopic lesions are not detected by conventional MRI, functional localization from symptoms is not clear, symptoms are missed at discharge, lesions become unclear in the chronic phase. Due to above reasons, neurobehavioral disability caused by TBI is called “invisible disability”, patients are often unable to obtain the understanding of families and others, and are sometimes unable to receive appropriate medical care.

The visualization of the anatomical lesions responsible for a neurobehavioral disability is essential for gaining an understanding of a patient’s clinical condition, making a diagnosis, and providing appropriate rehabilitation. In addition, changes in cerebral metabolism may be related in some way to a decline in cognitive

function following a TBI, and an investigation of such changes will contribute to clinicians' understanding of the patient's pathological condition.

In this study, I investigated the following subjects regarding TBIs with neurobehavioral disability. Chapter 1, deals with the question of whether it is useful to evaluate neuron loss by I-123 iomazenil single photon emission computed tomography (IMZ SPECT), as micro-brain damage is difficult to visualize by conventional MRI. In Chapter 2, the relationship between cerebral oxygen metabolism and cognitive function as examined by 15 O-labeled gas positron emission tomography (PET) is discussed.

List of Abbreviations

ASDH	acute subdural hematoma,
BAs	Brodmann areas
B–H	Benjamini–Hochberg
BP_{ND}	nondisplaceable binding potential
BZD	benzodiazepine
BZR	benzodiazepine receptor
CBV	cerebral blood volume
CT	computed tomography
DAI	diffuse axonal injury
DMN	default mode network
DV	distribution volume
DVR	distribution volume ratio
F	female
FDR	false discovery rate
FIQ	full intelligence quotient
FMZ	C-11 flumazenil
FWHM	full width at half maximum
GCS	Glasgow Coma Scale
IMZ	I-123 iomazenil
IQ	intelligence quotient
LPR	lesion-to-pons ratio
M	male,
MRI	magnetic resonance imaging
OEF	oxygen extraction fraction
PET	positron emission tomography
PIQ	performance intelligence quotient
RBMT	Rivermead Behavioural Memory Test
ROI	region of interest
SAH	subarachnoid hemorrhage
SD	standard deviation
SPECT	single photon emission computed tomography
TBI	traumatic brain injury
TEW	Triple energy windows
TIQ	total intelligence quotient
VIQ	verbal intelligence quotient
VOI	volume of interest

WAIS-Ⅲ	Wechsler Adult Intelligence Scale-Third Edition
WAIS-R	Wechsler Adult Intelligence Scale-Revised
WISC-Ⅲ	Wechsler Intelligence Scale for Children- Third Edition
WISC-R	Wechsler Intelligence Scale for Children-Revised

Chapter 1

Usefulness of I-123 Iomazenil Single Photon Emission Computed Tomography for Detecting Loss of Neuronal Integrity in Patients with Traumatic Brain Injury

Introduction

TBI cannot be explained only by the site of the brain injury detected by magnetic resonance imaging (MRI), it is difficult to diagnose neurobehavioral disability caused by TBI in many patients. The visualization of the lesions responsible for neurobehavioral disability is essential for understanding the clinical conditions, making a diagnosis, and providing appropriate rehabilitation. Several reports have shown that the loss of neuronal integrity could be detected using C-11 flumazenil (FMZ) positron emission tomography (PET) [8-13]. FMZ specifically accumulates in Benzodiazepine receptor (BZR). BZR forms a complex with the γ-aminobutyric acid type A ($GABA_A$) receptor (Figure 2) and is distributed throughout the brain cortex. It represents a reliable marker of neuronal integrity in various neurodegenerative diseases.

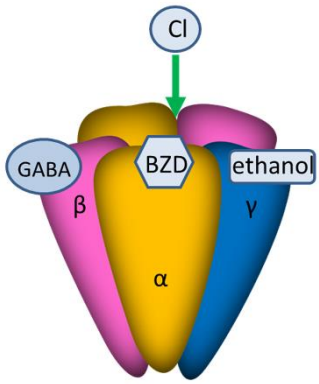

Figure 2. Scheme of $GABA_A$ receptor.
BZR forms a complex with the $GABA_A$ receptor.

In patients with ischemic cerebrovascular disorder, FMZ has been reported to be a useful marker indicating the presence of irreversible changes in neurons, even in a region where abnormalities were not found by MRI [9 8]. Several reports have shown that the loss of neuronal integrity in TBI patients can be evaluated by FMZ PET. We also have reported that TBI patients had low FMZ nondisplaceable binding potential (BP_{ND}) lesions indicating loss of neuronal integrity without MRI findings [12]. Moreover, in the FMZ PET of patients with diffuse axonal injury (DAI), abnormalities were observed in regions showing no abnormal MRI findings [13].

Similarly to FMZ PET, I-123 iomazenil (IMZ) single photon emission computed tomography (SPECT) can also be used to determine the distribution of the benzodiazepine receptor (BZR). IMZ SPECT has already been used clinically in many facilities for detecting epileptic foci in epilepsy patients (Figure 3).

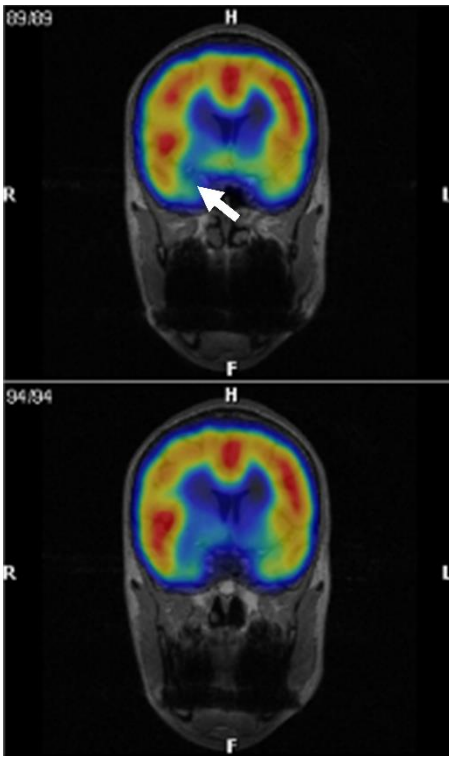

Figure 3. IMZ SPECT images in epilepsy. In this case, low benzodiazepine receptor area was found in the right temporal lobe.

Although IMZ is expected to show results similar to FMZ, IMZ is a SPECT tracer and FMZ is a PET tracer. Moreover, whereas the quantification method for FMZ PET has been established, quantification by IMZ SPECT is difficult and requires considerable efforts, thus limiting its use. To the best of our knowledge, there have been no studies in which FMZ PET findings and IMZ SPECT findings were compared in TBI patients, nor studies on whether those findings agree with each other.

The purpose of this study is to examine whether IMZ SPECT is as useful as FMZ PET for evaluating the loss of neuronal integrity in patients with neurobehavioral disability after TBI.

Materials and Methods

Patients

The subjects of this study were seven patients who suffered from neurobehavioral disability after TBI. The patients underwent FMZ PET, IMZ SPECT, and MRI.

Patient characteristics were shown in Table 1. TBI occurred at least 2 months (mean, 6 ± 5.6 months) previous to the time of FMZ PET and at least 6 months (mean, 17.7 ± 12.6 months) previous to the time of IMZ SPECT. The mean age of the patients was 30.3 years (standard deviation, 11.6 years). Of the seven patients, five were males and two were females. The causes of injury were traffic accident in five patients, assault in one patient, and sport-related in one patient. Epilepsy patients were not included in this study.

Table 1. Patient characteristics

Patient No.	Age (year)	Sex	WAIS-R, WAIS-Ⅲ,WISC-Ⅲ			RBMT	Diagnosis at the time of the accident	Period after injury (month)		Main symptoms
			FIQ	VIQ	PIQ			FMZ	IMZ	
1	28	M	98	105	90	21	no definite abnormalities	10	10	irritability, poor concentration
2	51	M	100	99	100	20	cerebral contusion	17	32	difficulty of calculation
3	39	M	104	111	94	16	no definite abnormalities	4	10	memory disorder
4	16	M	75	92	66	22	no definite abnormalities	2	13	memory disorder
5	21	M	90	98	105	17	cerebral contusion	2	6	mental fatigue
6	28	F	85	84	90	23	traumatic SAH, DAI, contusion	4	39	memory disorder
7	29	F	106	101	101	22	ASDH	3	14	mental fatigue

Ethics, consent, and permissions

The volunteers gave their written, informed consent in accordance with the Helsinki II declaration, and this study was approved by the Ethics Committees of Hokkaido University Graduate School of Medicine.

PET

Images were acquired with a 5-min transmission scan and a 60-min dynamic emission scan with the HR+ PET scanner (Asahi-Siemens, Tokyo, Japan) (Figure 4) in the 3D acquisition mode, and images were reconstructed with the brain mode of manufacturer's software. The energy window was 350–650 keV. The acquired 3D sinograms were converted into 2D sinograms with the Fourier rebinning algorithm. The images were reconstructed by directinversion Fourier transformation. The reconstruction filter was a Hanning filter with 4-mm FWHM. The reconstruction matrix was 256 × 256, and the FOV was 33 cm in diameter. The full width at half-maximum (FWHM) was 6.4 mm after reconstruction. FMZ PET procedures were the same as previously described [9].

Dynamic FMZ PET was performed on all the patients (Figure 5). The drugs that affect BZR were withdrawn at least 1 week before FMZ PET studies. The injected dose of FMZ was 370 MBq for each patient. A set of 27 sequential PET frames of increasing duration were obtained over 60 min after FMZ injection, according to the following protocol: 40 s × 1 frame, 20 s × 10 frames, 60 s ×4 frames, 180 s × 4 frames, and 300 s × 8 frames.

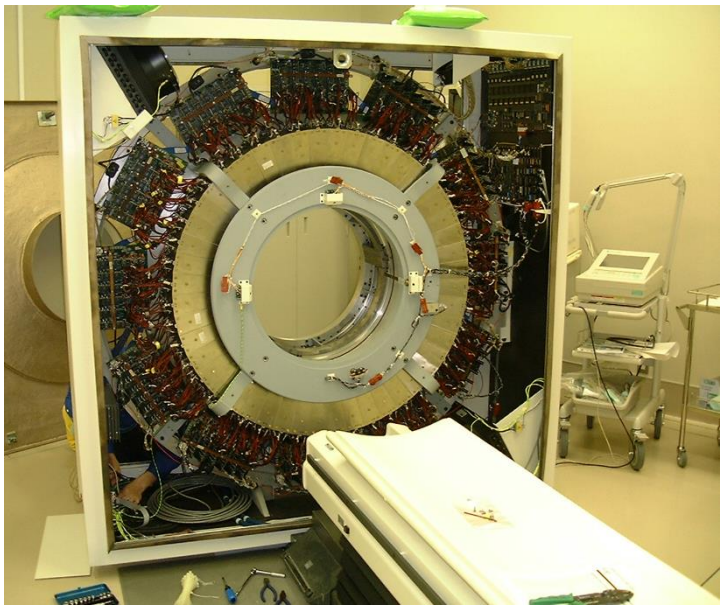

Figure 4. PET. Images were acquired with the HR+ PET scanner (Asahi-Siemens, Tokyo, Japan).

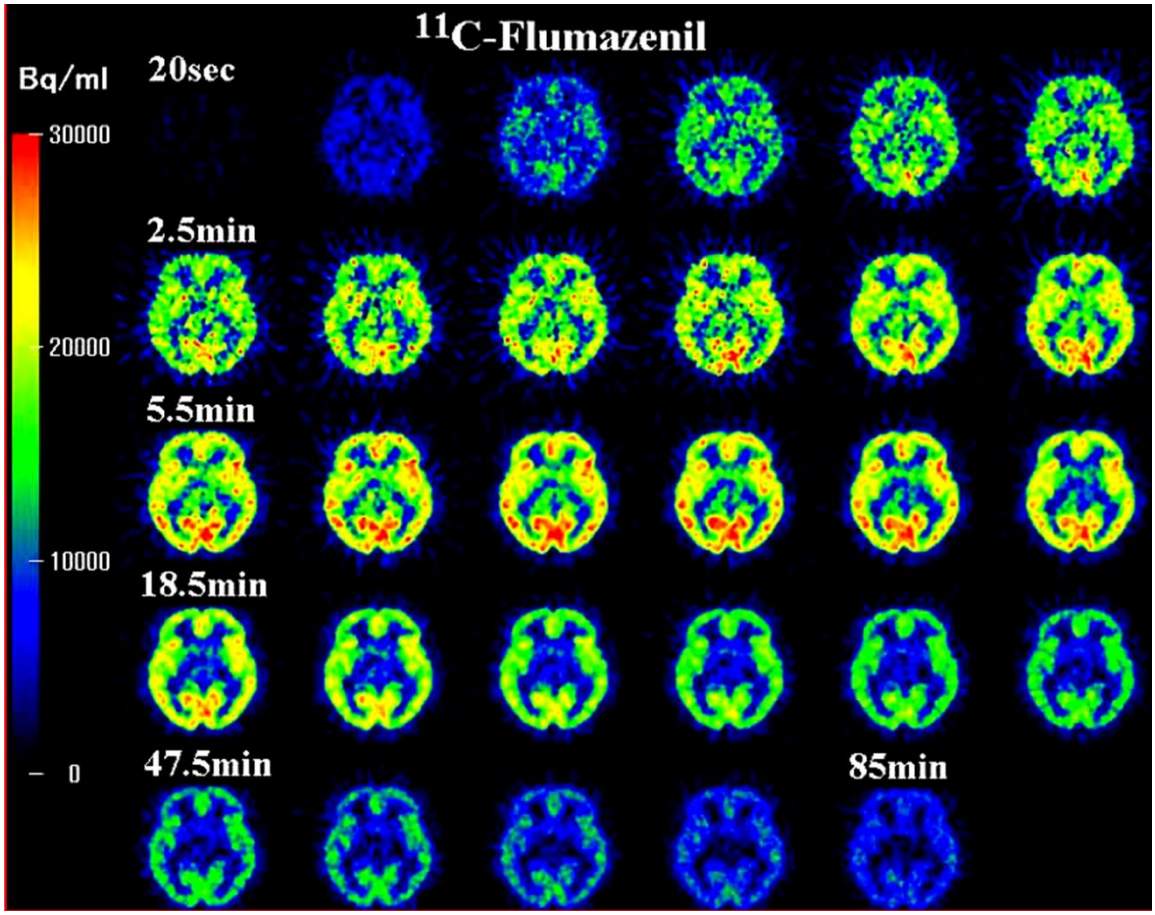

Figure 5. Dynamic FMZ PET images. FMZ PET images in the early phase are regarded to be strongly influenced by blood perfusion, whereas those in the late phase are considered to be affected by receptor binding.

A reference tissue compartment model was used for a noninvasive estimation of BP_{ND} with a time-activity curve in the pons as an indirect input function (Figure 6).

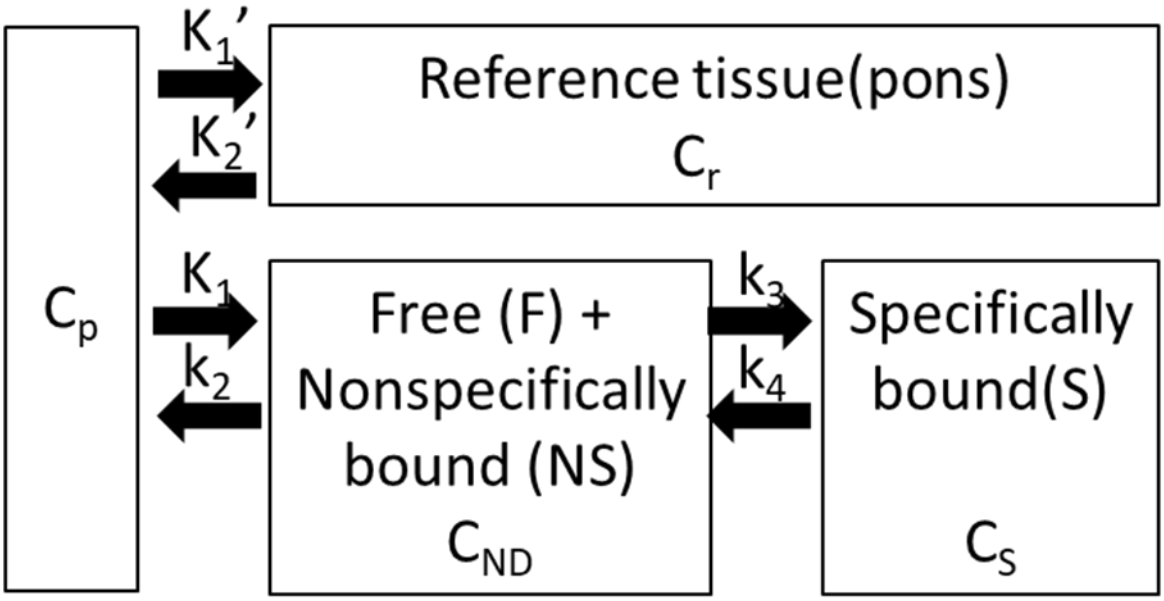

Figure 6. Reference tissue model, with a two-tissue compartment model for the target region and a single-tissue compartment model for then reference region.

$dC_{ND}/dt = K_1 C_p - k_2 C_{ND} - k_3 C_{ND} + k_4 C_S$ ----(1)
$dC_S/dt = k_3 C_{ND} - k_4 C_S$ ----(2)
$dC_r/dt = K_1' C_p - k_2' C_r$ ----(3)
$K_1'/k_2' = K_1/k_2$ ----(4)
$BP_{ND} = k_3/k_4$ ----(5)

C_p is the metabolite-corrected plasma concentration (kBq/mL), C_r is the concentration in reference tissue (kBq/mL), C_{ND} is the concentration of nondisplaceable (free plus nonspecifically bound) ligand (kBq/mL), C_S is the concentration of specifically bound ligand (kBq/mL), K_1 is the rate constant for transfer from the plasma to nondisplaceable compartment (mL/g/min), k_2 is the rate constant for transfer from the free to the plasma compartment (/min), k_3 is the rate constant for transfer from the nondisplaceable to the bound component (/min), k_4 is the rate constant for transfer from the bound to the nondisplaceable compartment (/min), K_1' is the rate constant for transfer from the plasma to the reference compartment (mL/g/min), k_2' is the rate constant for transfer from the

reference to the plasma compartment (/min), and t is time (min). The operational equation can be further simplified by assuming that the volume of distribution of the nonspecifically bound tracer in both tissues is the same as that obtained using Eqs.(4). Finally, BP_{ND} was estimated by the nonlinear least method using Lammertsma's simplified reference tissue model[14]. The parametric images were calculated with the program developed in our institute using Microsoft Visual C++ 6.0 for Windows.

SPECT

The dose of iodine-123 IMZ was 167 MBq. SPECT data were acquired from 20 to 40 min and 120 to 140 min after the tracer injection, using a triple-head gamma camera (GCA-9300/DI, TOSHIBA, Tokyo, Japan) equipped with low-energy high-resolution fan-beam collimators (Figure 7). The latter images were used for analysis because delayed IMZ SPECT activity and distribution volume of IMZ SPECT had high linear correlation[15]. The energy settings were 160 keV peak with 24% width. The matrix size was 128 × 128 pixels. The images were reconstructed using the filtered back-projection method without scatter correction. The data were pre-processed using a Butterworth filter with a cutoff frequency of 0.10 cycles per pixel and a power factor of eight. Attenuation correction was performed using Chang's method. The attenuation coefficient was set at 0.10/cm. These attenuation coefficient values were determined by a phantom study. The imaging resolution was about 10 mm full width at half-maximum (FWHM) after reconstruction. Table 2 shows image acquisition and correction methods of FMZ PET and IMZ SPECT study.

Figure 7. SPECT. SPECT data were acquired using a triple-head gamma camera (GCA-9300/DI, TOSHIBA, Tokyo, Japan).

Table 2. Image acquisition and correction methods of FMZ PET and IMZ SPECT study

	FMZ PET study	IMZ SPECT study
Tracers	C-11 flumazenil	I-123 iomazenil
Acquisition system	BGO PET system (Asahi-Siemens ECAT EXACT HR+)	Triple-head gamma camera with low energy high resolution fan-beam collimators (Toshiba GCA-9300)
Scatter correction	Single scatter simulation method	No scatter correction
Attenuation correction	Measured with transmission scan	Chang's method
Reconstruction method	Fourier rebinning algorithm + Direct-inversion Fourier transformation	Filtered back projection
Image acquisition	60 minute dynamic acquisition with 3D mode	Static image (20 to 40 minutes and 120 to 140 minutes after the tracer injection)
FWHM (mm) after reconstruction	6.4	10

MRI

MRI scan was performed using a 1.5 Tesla scanner (Magnetome Vision or Magnetome Symphony, Asahi-Siemens, Tokyo, Japan). Transaxial T2 and T2* weighted images and FLAIR images were acquired. All images were acquired with 5-mm slice thickness and no slice gap. Coronal and sagittal images were added in some cases.

Data analysis

The images obtained were assessed visually and semiquantitatively. As described previously, FMZ PET and delayed IMZ SPECT images were automatically superimposed on MRI images using multimodality image registration techniques [16] . The locations of low-uptake-level regions on FMZ PET and delayed IMZ SPECT

images were visually assessed in three directions (Figure 8). Two specialists in nuclear medicine interpreted the images independently. When their findings did not agree, the presence or absence of low-uptake-level regions was determined by discussion.

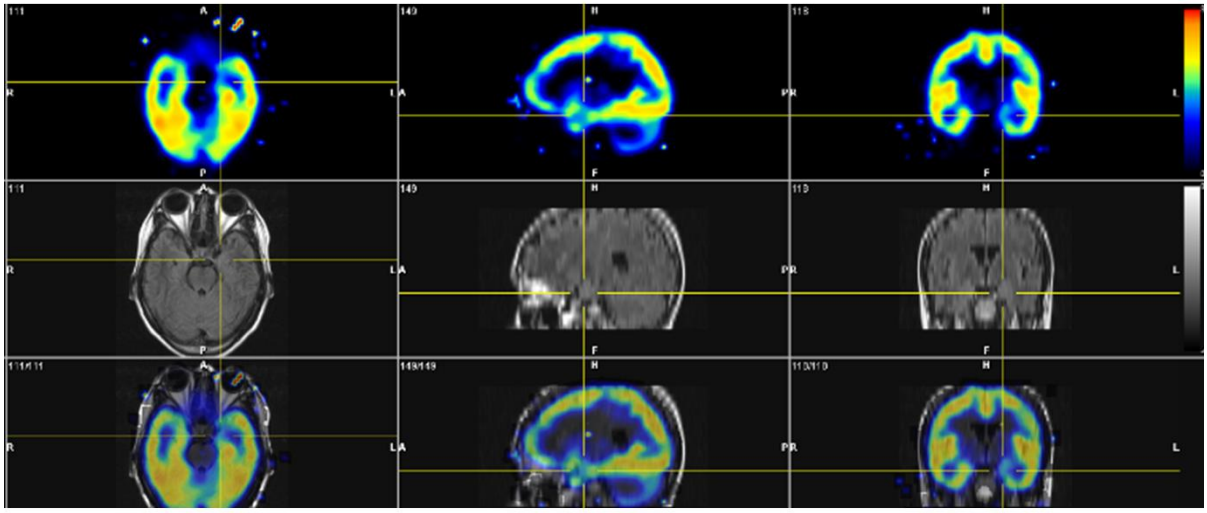

Figure 8. Co-registration to MRI. In this case, the low uptake level is observed at the light temporal lobe.

A region of interest (ROI) was placed in the lesions, which was visually detected on FMZ PET images. The ROI was circle shaped of 9 mm in diameter. In delayed IMZ SPECT, a same ROI was placed in the lesion detected in FMZ BP_{ND}, and the uptake of IMZ in the ROI was evaluated. The uptake of delayed IMZ was evaluated on the basis of lesion-to-pons ratio (LPR), which was corrected using the pons as the reference region. LPR can be expressed as follows:

$$LPR = \frac{delayed\ activity\ (ROI)}{delayed\ activity\ (Refarence)} \quad (6)$$

On the other hand, the distribution volume (DV) in the equilibrium state of Figure 6 can be expressed as equation (7). BP_{ND} can indirectly calculated as shown in equation (8) described by Innis et al[17] [18]. The term DV_T/DV_{ND} is termed the distribution volume ratio (DVR) (9). And DVR is DV value relative to that of the reference tissue [19] (10). LPR corresponded to DVR of IMZ because delayed IMZ SPECT activity and distribution volume of IMZ SPECT had high linear correlation (10)(11)[15].

$$DV_T = DV_{ND} + DV_S \quad (7)$$

$$BP_{ND} = \frac{V_T - V_{ND}}{V_{ND}} = \frac{V_T}{V_{ND}} - 1 \quad (8)$$

$$= DVR - 1 \qquad (9)$$

$$= \frac{DV(ROI)}{DV(Refarence)} - 1 \qquad (10)$$

$$= \mathrm{LPR} - 1 \qquad (11)$$

DV_T is the total distribution volume of radioligand in tissue (mL/cm^3), DV_{ND} is the distribution volume of nondisplaceable radioligand (mL/cm^3), DV_S is the distribution volume of specifically bound radioligand (mL/cm^3).

We compared FMZ BP_{ND} and (LPR-1) of delayed IMZ SPECT (Figure 9). The significant difference was determined by the paired t test and Pearson's correlation coefficient to examine the relationship between these two parameters. A difference of $p < 0.05$ was determined as significant.

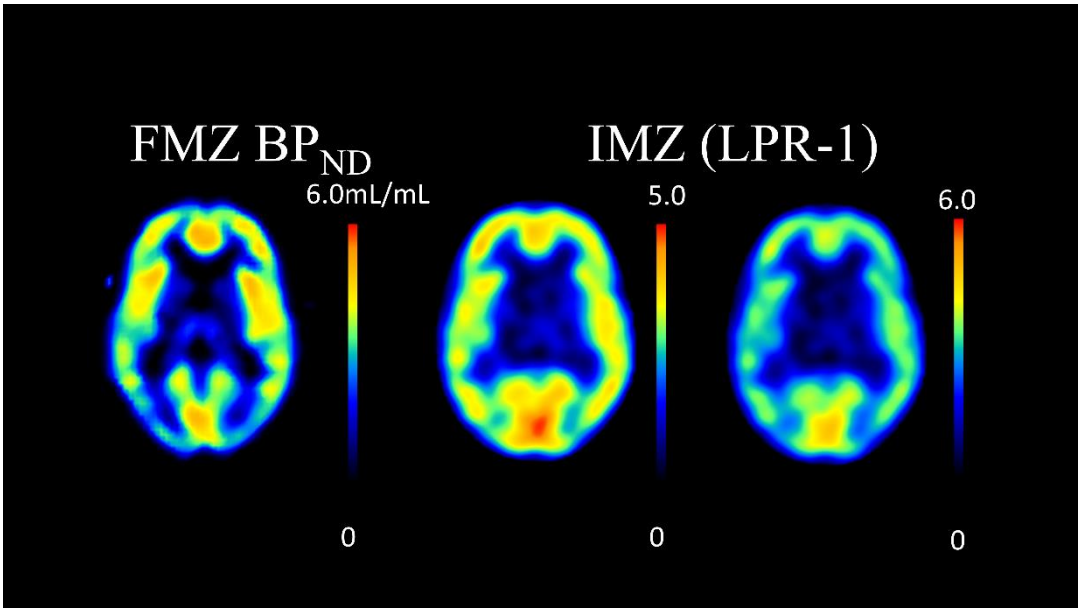

Figure 9. Parametric images of FMZ PET and IMZ SPECT. Left is FMZ BP_{ND} (0–6.0 mL/mL). Center image is IMZ (LPR-1) ranging from 0 to 5.0. Right image is IMZ (LPR-1) ranging from 0 to 6.0.

Results

Table 1. shows the diagnosis given at the time of injury, the period after injury, the main symptoms, the scores on the Wechsler Adult Intelligence Scale-Revised (WAIS-R) [20], Wechsler Adult Intelligence Scale-Third Edition (WAIS-III) [21], or the Wechsler Intelligence Scale for Children-Third Edition (WISC-III) [22], and the results of the Rivermead Behavioural Memory Test (RBMT). None of the patients

showed clear focal neurological dysfunction. The WAIS scores were at or below the cutoff point in two patients. Two patients had scores at or below the cutoff point in RBMT. The main symptoms were memory disorder in three patients, mental fatigue in two patients, difficulty of calculation and irritability in one patient, and irritability in one patient.

A decrease in FMZ BP_{ND} was visually detected in 11 regions. In delayed IMZ SPECT images, low uptakes were observed in nine lesions, eight of which also showed decreases in FMZ BP_{ND}. The rate of concordance between FMZ PET and delayed IMZ SPECT was 72.7%. One lesion not detected by FMZ PET was detected by delayed IMZ SPECT (Table 3.). Representative cases are shown in Figures. 10, 11, and 12.

Table 3. Findings in the seven patients with respect to location of low FMZ BP and location of low uptake levels on IMZ images

No.	MRI		Location of low uptake on FMZ images	Location of low uptake on IMZ images
1	DAI (microbleeds)	Rt parietal lobe Lt temporal lobe	Rt medial temporal lobe	Rt medial temporal lobe
2	Contusion	Rt temporal tip Bilateral frontal lobes	Rt medial temporal lobe Lt frontal tip	Rt medial temporal lobe
3	none		Lt basal-medial temporal lobe	Lt medial temporal lobe
4	DAI (microbleeds)	Lt frontal lobe Lt parietal lobe Bilateral cerebella	Rt medial temporal lobe Lt frontal tip	Rt basal-medial temporal lobe
5	DAI (microbleeds)	Bilateral frontal lobes Bilateral temporal lobes	Lt frontoparietal lobe	Lt frontoparietal lobe Rt basal-medial temporal lobe
6	DAI (microbleeds)	Bilateral frontal lobes Bilateral internal capsule	Rt basal-medial temporal lobe	Rt basal-medial temporal lobe
7	DAI (microbleeds)	Lt frontal Lt temporal Lt brain stem	Rt basal temporal lobe Lt frontal tip Lt frontoparietal lobe	Rt basal-medial temporal lobe Lt frontal tip

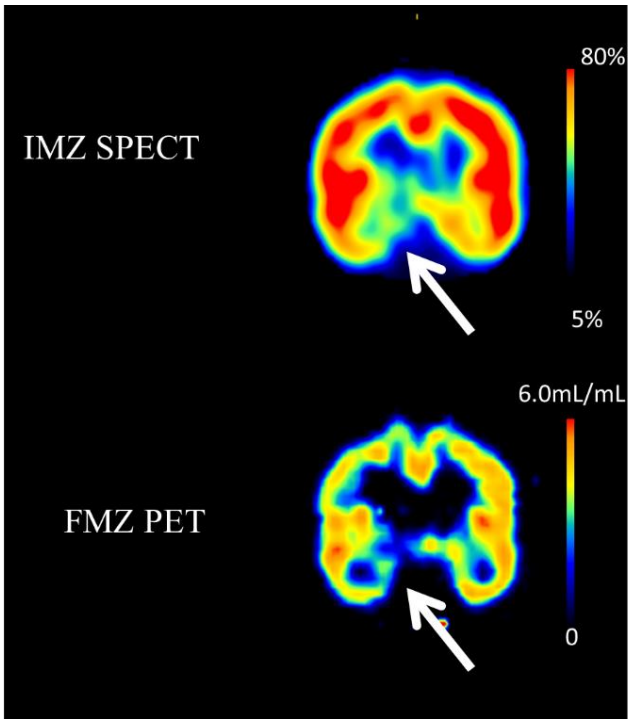

Figure 10. Case 1 (Patient No. 1): The patient was a 28-year-old male who was injured in a car accident 1 year previously. No abnormalities were found at the time of injury but he complained of irritability and poor concentration after the injury. Microbleeds in the right parietal lobe and left temporal lobe were observed on MRI images in the chronic phase. FMZ BP was low inside the right temporal lobe. The low uptake level inside the right temporal lobe was also observed by IMZ SPECT.

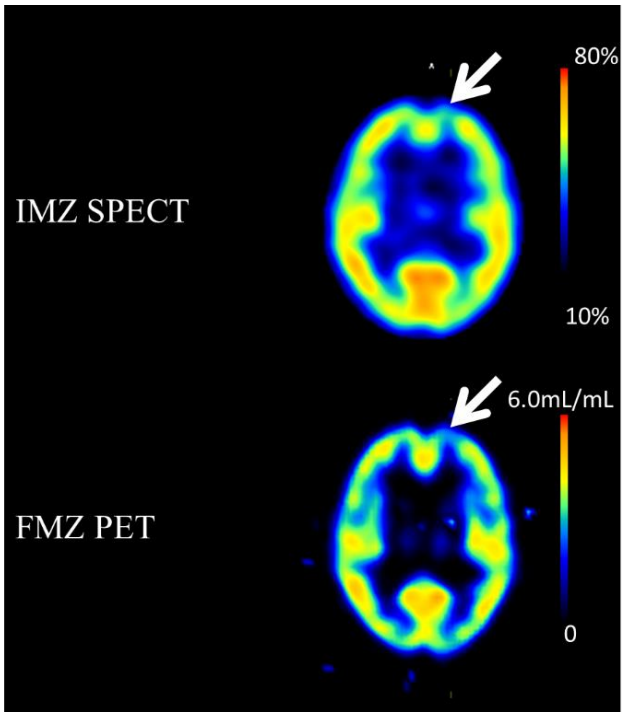

Figure 11. Case 2 (Patient No. 7): The patient was a 29-year-old female who was diagnosed as having acute subdural hemorrhage at the time of injury and complained of mental fatigue and headache after the injury. FMZ BP_{ND} was low inside the left frontal lobe. The low uptake level inside the left frontal lobe was also observed by IMZ SPECT.

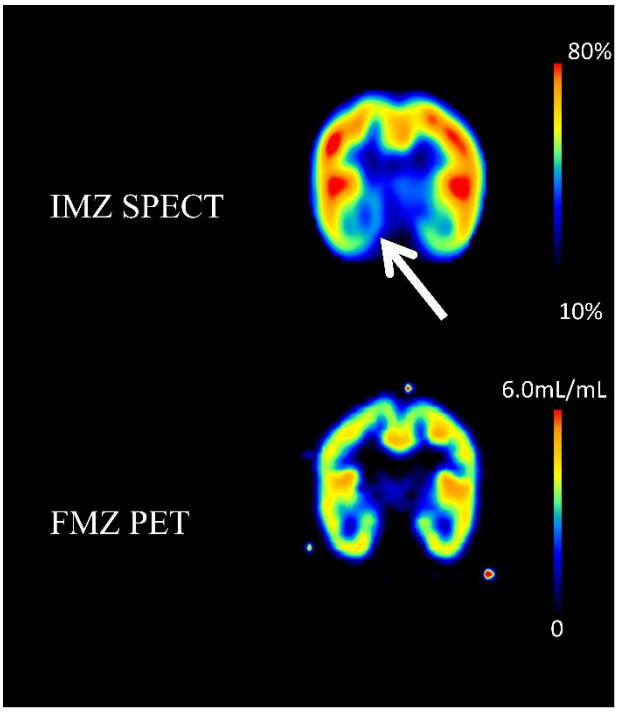

Figure 12. Case 3 (Patient No. 5): The patient was a 21-year-old male who was diagnosed as having right frontal brain contusion at the time of injury and complained of mental fatigue after the injury. The uptake level of IMZ SPECT was low at the right basal-medial temporal lobe. But the low BP_{ND} was not observed by FMZ PET.

The (LPR-1) of IMZ SPECT in the 11 lesions which were detected with FMZ PET was significantly lower than FMZ BP_{ND} (Figure 13). There was significant correlation between FMZ BP_{ND} and IMZ (LPR-1) ($p = 0.003$). The correlation coefficient (r) between FMZ BP_{ND} and IMZ (LPR-1) was 0.80, indicating a strong positive correlation between the two (Figure 14).

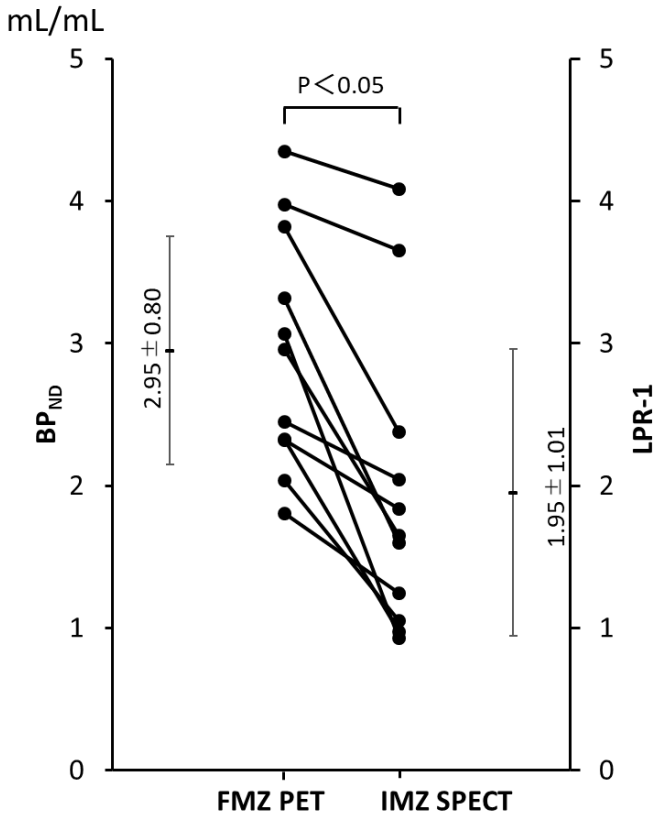

Figure 13. The (LPR-1) of IMZ SPECT in the 11 lesions which were detected with FMZ PET was significantly lower than FMZ BP_{ND}.

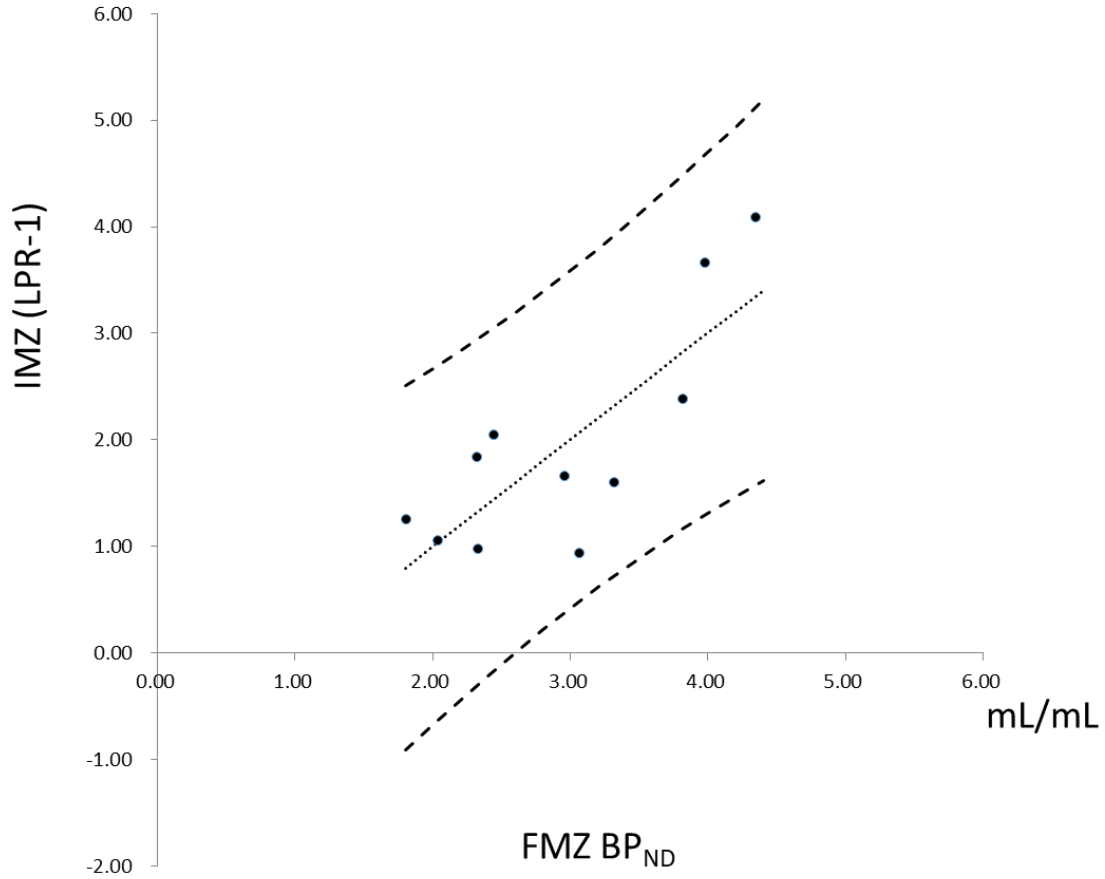

Figure 14. A positive correlation was found by Pearson's correlation coefficient between the BP_{ND} in the lesions detected by FMZ PET and the (LPR-1) in the same regions obtained in IMZ SPECT (r^2 =0.638).

Discussion

When FMZ BP_{ND} image was used as the reference, eight of 11 lesions were detected by IMZ SPECT. That is, most of the lesions were detected by IMZ SPECT. The sensitivity of FMZ PET in detecting lesions was slightly higher than that of IMZ SPECT. However, a lesion that was not detected by FMZ PET was detected by IMZ SPECT. IMZ (LPR-1) correlated with FMZ BP_{ND} but was significantly lower than FMZ BP_{ND}.

In this study, FMZ PET and IMZ SPECT were used to identify the loss of neuronal integrity. Both FMZ and IMZ are tracers that specifically bind to central BZR. Central BZR forms a complex with the $GABA_A$ receptor and is distributed throughout the brain cortex.

It has been reported that a low IMZ uptake level correlates with decreased neuronal density in epilepsy patients [11] [10] ; and IMZ has already been used for epilepsy diagnosis in clinical practice.

Several reports have shown that the loss of neuronal integrity in TBI patients can be evaluated by FMZ PET [12] [13]. We have reported that even in patients with head injury showing no abnormal MRI findings, regions with a decreased cerebral metabolic rate of oxygen ($CMRO_2$) were identified by O-15-labeled gas PET, and that a decrease in BP_{ND} was observed on FMZ PET images in some of those regions. The decrease in FMZ BP_{ND} may be related to the loss of neuronal integrity, and it seemed that the decrease in $CMRO_2$ in the regions showing no loss of neuronal integrity was due to functional hypometabolism [12].

FMZ PET and IMZ SPECT are considered to be useful for identifying the loss of neuronal integrity. However, a comparison between FMZ PET and IMZ SPECT in epilepsy patients showed that FMZ PET more accurately detects epileptic foci, whereas the accuracy of IMZ SPECT was lower [23]. There has been no report that FMZ PET findings and IMZ SPECT findings agree with each other in TBI patients. In this study, most of the IMZ SPECT findings agreed with the FMZ PET findings, suggesting that IMZ SPECT was as useful as FMZ PET for evaluating the loss of neuronal integrity in TBI patients. However, it should be noted that the IMZ SPECT and FMZ PET findings were not completely identical because of the inherent differences between the tracers (FMZ and IMZ) and image generation methods; PET v.s. SPECT.

Inherent differences between PET and SPECT and their tracers

The direction of gamma rays is determined by a collimator in SPECT. PET can determine photon origin using coincidence detection, it does not require a collimator. A collimator attenuates large number of incoming radiation; therefore, PET has an increase in sensitivity of two to three orders of magnitude compared to PET. PET has excellent performance in resolution and sensitivity [24]. Moreover, PET is superior to SPECT in quantitative performance because absorption is directly measured in PET, or calculated by CT in PET/CT, whereas that in SPECT is only corrected using a mathematical model (Chang's method). FMZ PET, which has a high spatial resolution, is more accurate than IMZ SPECT because abnormalities are determined on the basis of the visual assessment of low-uptake-level regions. To address the issue of spatial resolution, a high sensitivity SPECT system was used in this study. This may be the reason why the accuracy of IMZ SPECT in this study was higher than that of the report on the comparison of FMZ PET and IMZ SPECT in epilepsy patients [23].

FMZ is an antagonist of BZR [25]. In the brain, 80– 90% of FMZ specifically binds to BZR and the rest exists as free or nonspecifically bound FMZ [26-28]. Moreover, the quantification method for FMZ PET has been established. FMZ is taken up by the brain immediately after its injection and is then promptly washed out. Quantitative values can be obtained by 1-h dynamic scanning immediately after the injection of FMZ. IMZ is a partial inverse agonist. The BZR affinity of IMZ is 10fold that of FMZ, and the specific-to-nonspecific binding ratios are 40–50:1 [29 30]. The quantification method for IMZ SPECT has not been established. FMZ PET BP_{ND} images are quantitative images that can exclude nonspecific accumulation. On the other hand, IMZ SPECT images are qualitative images that cannot exclude nonspecific accumulation, leading to decreased contrast and decreased sensitivity for detecting abnormalities. In contrast, IMZ is an agonist, unlike FMZ, having pharmacological effects. IMZ is designed as a tracer that has low ligand occupation rate because of pharmacological effect.

The accumulation of LPR in IMZ SPECT was determined in this study. The reference tissue for FMZ BP_{ND} is the pons, which shows little specific accumulation of BZR. Therefore, the accumulation LPR as determined by IMZ SPECT was compared with the quantitative value obtained by FMZ PET. This may be the reason why the semiquantitative accuracy of IMZ SPECT was improved and the IMZ (LPR-1) showed a high level of correlation with FMZ BP_{ND}. Table 4 shows differences between PET and SPECT and their tracers.

Table 4. Differences between PET and SPECT and their tracers

	FMZ PRT	IMZ SPECT
Acquisition system	Determine photon origin using coincidence detection.	Determine direction of gamma rays using collimator which attenuates incoming radiation.
Correction	Directly measured	Mathematical model.
Tracers	Antagonist (no pharmacological effects)	Partial inverse agonist (low ligand occupation rate because of pharmacological effects)
Imaging	Quantitative images that can exclude nonspecific accumulation	Qualitative images that cannot exclude nonspecific accumulation

Decrease in expression level of BZR

There are three possible causes of a decrease in BZR expression level. The first is direct injury. Brain contusion is often located at the bottom, outer surface, and inner surface of the frontal and temporal lobes, or in the temporal pole [31]. In this study, all the regions showing a decrease in BZR expression level were located in the frontal and temporal lobes, with most of them located at the bottom, inside, and in the pole of these lobes. The injuries seemed to have been caused by the bone of the skull base.

The second is DAI. DAI is an axonal injury due to the shear or distortion induced by rotational acceleration and is often located at the corticomedullary junction or in deep white matter [32] [33]. It has been reported that an axonal injury slowly leads to Wallerian degeneration and results in delayed neuronal death [34]. Although BZR is not suitable for detecting disorders in the white matter because it exists in the gray matter, the abnormalities detected may indicate neuronal death caused by DAI. In this study, five patients had DAI identified by MRI.

The third is apoptosis. Apoptosis was observed in the injured brain cortex and white matter in a study using mild TBI models, indicating that TBI was a cause of cell death [35].

In this study, there was a region where abnormalities were detected only by IMZ SPECT. Such abnormalities may be a false positive resulting from the limited resolution of SPECT and the issues of accuracy of the test method such as the lack of quantification. Moreover, the results may be affected by the difference in the time point at which FMZ PET and IMZ SPECT were carried out.

In this study, IMZ SPECT was carried out several months after FMZ PET. Therefore, there was a possibility that secondary changes due to TBI, including Wallerian degeneration and apoptosis, led to the decrease in BZR expression level, and, as a result, the abnormalities not detected by FMZ PET were detected by IMZ SPECT. Further research is required to clarify the temporal changes detected by IMZ SPECT.

Correlation of FMZ BP_{ND} and (LPR-1) of IMZ

We compared FMZ BP_{ND} and (LPR-1) of delayed IMZ SPECT. In previous study, BP_{ND} of IMZ SPECT were much higher than (LPR-1). If IMZ binds about 10 times as strong as FMZ, (LPR-1) will be 10 times larger than BP_{ND} of FMZ. Millet et.al reported that BP_{ND} of IMZ was about 5 times that of FMZ. Considering that the spatial resolution of SPECT is worse than that of PET, BP_{ND} of IMZ is considered to be higher than that of FMZ by more than 5 times. One reason was considered to be derived from scatter correction. We did not correct the scatter in SPECT study.

This SPECT system is equipped with Triple energy windows (TEW) scatter correction. Because the TEW method was reported to increase the noise [36] and visual interpretation was difficult in some cases, we decided to analyze SPECT images without scatter correction. Scatter correction is important in the quantitative analysis of brain SPECT. Skull base has high attenuation [37] and therefore generates a lot of scatter photons. Axelsson et al. [38] reported that the relation between true and measured concentration ratios was almost linear after scatter correction and the effect of scatter correction was larger in the low counts area than in the high counts area. The activity of pons might be overestimated in this study. Other reason was derived from static data acquisition. We did not perform dynamic study in SPECT. Dynamic study was necessary to calculate accurate DV and BP in both PET and SPECT study. Other reason was derived from attenuation correction. Absorption correction of PET is based on mu map directly measured in PET, or calculated by CT in PET/CT, and it was more accurate than that of SPECT system.

Clinical significance of IMZ SPECT

Cerebral blood flow SPECT is more sensitive to TBI associated dysfunction than MRI and computed tomography (CT) [39] [40]. However, blood flow and glucose metabolism change in connection with the activities of the patient examined and therefore reflect even a functional decline that is not due to a neuronal abnormality. The neuron loss can be more accurately detected using BZR-specific ligands.

It is considered that FMZ PET has higher diagnostic accuracy than IMZ SPECT. However, 11C-FMZ must be purified in a hospital because its half-life is as short as 20 min. It can be used only for research purposes and is difficult to use in clinical settings. On the other hand, IMZ has long radioactive half-life, it is easy to handle it. And it can be used in many facilities because it is more easily available than FMZ.

Limitations

The number of patients involved in this study was small. Further research with a larger number of patients is required in the future.

As for PET system, we used Siemens HR+ PET system for FMZ PET study. HR+ PET system was a high spatial resolution BGO PET system (The special resolution at the 1 cm point in the vertical direction from the center defined by the NEMA NU-2001 standard was 4.39.) and with relatively high sensitivity (The sensitivity defined by the NEMA NU-2001 standard was 6.65kps/MBq in the case of the energy lower limit 350KeV). We think that this system was still good only for brain

study; however, it seemed to be old system in these days. It had no CT system and lower energy resolution (23%) than LSO or LYSO system (10–14%). State-of-the-art time-of-flight PET/CT system is better for further analysis.

As for SPECT system, we used triple-head gamma camera. Triple-head gamma camera with fan-beam collimator had high spatial resolution with high sensitivity. Our results might be attributed to these features of triple-head gamma camera. As two-head gamma cameras are prevalent these days, the results might not be universal.

We did not correct scatter in SPECT study. New scatter corrections without increasing noise were developed [41]. With those scatter corrections, the correlation of semiquantitative parameters of PET and SPECT might become better without affecting visual diagnosis.

Chapter 2
Relationship between Cognitive Function and Cerebral Oxygen Metabolism in Traumatic Brain Injury Patients with Neurobehavioral Disability

Introduction

O-15-labeled gas PET is a neuroimaging technique to easily quantify cerebral metabolism. Changes in cerebral metabolism may be related in some way to cognitive function decline following TBI.

There have been many reports on cerebral metabolism in TBI patients with cognitive function decline. We previously reported the decrease in cerebral metabolic rate of oxygen ($CMRO_2$) in certain brain areas and also a decrease in binding potential (BP) in some of those areas detected by FMZ PET, even in patients with TBI without MRI abnormal findings. It was considered that a decrease in FMZ BP is related to neuronal loss and that a regional decrease in $CMRO_2$ in the areas without neuronal loss indicates functional hypometabolism[12].

In previous PET studies of patients with TBI, it was found that hypometabolism or hypermetabolism occurred in the frontal lobe (Table 5) [42-48] . The prefrontal area plays a key role in high-level cognitive function and is considered to be related to neurobehavioral disability following TBI. Although the classification of the prefrontal area varies depending on the literature, the area is roughly divided into three parts, namely, the lateral prefrontal cortex, orbitoprefrontal cortex, and medial prefrontal cortex[49].

Table 5 Published PET studies on metabolism of TBI patients

references	drug	state of subject	cases	summary
Humayun et al.,1989	FDG	vigilance task	3	Increases: medial temporal cortex; frontal cortex Decreases: lateral temporal cortex; caudate nucleus
Gross et al.,1996	FDG	performance task	20	Increases or Decreases: midtemporal; anterior cingulate; precuneus; anterior temporal frontal lobe; corpus callosum
Ruff et al.,1994	FDG	resting	9	Decreases: frontal; anteriotemporo-frontal
Umile et al.,2002	FDG	resting	20	Abnormalities: temporal lobe
Kato et al.,2007	FDG	resting	36	Decreases: frontal; temporal thalamus; cerebellum
Provenzano et al.,2010	FDG	resting	19	Decreases: posterior cingulate cortex; parieto-occipital; frontal lobes; cerebellum
Peskind et al.,2011	FDG	resting	12	Decreases: cerebellum; vermis; pons; medial temporal lobe

The orbitoprefrontal cortex plays an important role in emotion and motivation whereas the medial prefrontal cortex plays an important role in psychosocial and social functioning. The lateral prefrontal cortex is the seat of cognitive and executive functions. Some studies on healthy subjects and patients with certain disorders suggest that the lateral prefrontal cortex is related to general intelligence [50-53].

WAIS is the most common test used to assess general intelligence and is often used for patients with neurobehavioral disability following TBI in clinical practice and research. Although verbal IQ (VIQ) and performance IQ (PIQ) can be assessed separately with WAIS, their reliability and validity were low in patients with unilateral brain injury [54 55]. It was pointed out that a discrepancy of more than 10 between VIQ and PIQ was common in healthy subjects [56]. Because of the low validity and other problems of separately assessed VIQ and PIQ, the VIQ and PIQ subsets are not used in the latest revised version Forth Edition (WAIS-Ⅳ). The total IQ (TIQ) of WAIS-Revised (WAIS-R) indicates the general intelligence level.
The purpose of this study is to investigate the relationship between cerebral metabolism and cognitive decline in TBI patients. We examined the relationship between $CMRO_2$ in the lateral prefrontal cortex measured by O-15-labeled gas PET and TIQ in TBI patients with neurobehavioral disability.

Materials and Methods

Subjects

The subjects were 12 patients (8 males and 4 females) who had difficulties in their daily life and work because of some forms of neurobehavioral disability following TBI. Their mean age was 33.3 years [standard deviation (SD), 14.83 years]. The cause of injury was traffic accidents in all patients and the mean period after injury was 44.8 months (SD, 37.2 months). None of the patients had epilepsy.

Neurological test

Cognitive function was assessed using the Wechsler Intelligence Scale for Children-Revised (WISC-R) in one patient aged younger than 16 years and WAIS-R in the remaining 11 patients. Table 6 shows the results and patient characteristics.

Table 6. Patient characteristics

No.	age (year)	sex	period after injury (month)	location of hypometabolism on $CMRO_2$ images	chief complaint	TIQ
1	22	M	60	diffuse	irritability	64
2	34	F	30	diffuse, especialiy Lt temporal lobe	memory disorder	88
3	28	M	136	Rt medial temporal	memory disorder	79
4	55	M	14	Bil temporal	irritability	114
5	24	M	48	Bil frontal,Bil temporal lobe	diminished thinking ability	117
6	55	F	5	diffuse,especialiy Bil frontal, temporal lobe	loss of concentration	109
7	55	F	9	Rt temporal lobe	loss of concentration	113
8	24	M	93	Bil frontal,Bil temporal Rt parietal lobe Rt thalamus	irritability	106
9	24	M	52	Rt frontal,Rt temporal lobe	irritability	55
10	46	M	33	Bil. Frontal ,temporal	memory disorder	102
11	21	M	50	Rt frontal white matter	irritability	85
12	11	F	7	Lt frontal,Rt temporal～occipital lobe Rt cerebellum(crossed cerebeller diaschisis)	memory disorder	72

PET

PET was performed using ECAT EXACT HR + (Asahi-Siemens, Tokyo, Japan) with in-plane and axial resolutions of 4.5 and 3.71 mm, respectively. Photon attenuation was corrected with a 5 min transmission scan. O-15-labeled gas PET and FMZ PET procedures were the same as previously described [9].

O-15-labeled gas PET

A one-minute inhalation of ^{15}O-CO and 3-minute static scanning and blood sampling were performed to measure cerebral blood volume (CBV). A steady state CO_2 image was scanned for 5 minutes with a 15-minute inhalation of 7.5GBq ^{15}O - CO_2 and arterial blood and plasma sampling. With a 15-minute inhalation of ^{15}O - O_2, a steady-state O_2 image was scanned for 5 minutes and arterial blood and plasma were sampled to measure oxygen extraction fraction (OEF) and the cerebral metabolic rate of oxygen ($CMRO_2$). PaO_2 and $PaCO_2$ and the blood pH were also measured in the same blood samples. Regional cerebral metabolism was investigated on the basis of $CMRO_2$ images.

$CMRO_2$ images were spatially normalized using PET template with SPM5. Spatially normalized PET images were smoothed by 12 x 12 x 12 Gaussian kernel. Following spatial normalization, volume of interest (VOI) extraction for the cerebellar cortex was performed in every $CMRO_2$ image using the WFU Pick Atlas toolbox (Wake Forest University School of Medicine, Winston-Salem, NC, USA).

We investigated the correlation between $CMRO_2$ of lateral prefrontal cortex (Brodmann area 9,44,45,46,47) and TIQ.

Analysis

Pearson's correlation was calculated and assessed with a significance level of 5%. For multiple-test corrections, the Benjamini–Hochberg (B–H) procedure was used to control false discovery rate (FDR) at <0.05.

Results

Table 6 shows the period after injury, locations of hypometabolism on $CMRO_2$ images, chief complaints, and TIQ of WAIS-R in each patient. The chief complaints were irritability in five patients, memory disorder in four patients, loss of concentration in two patients, and diminished thinking ability in one patient. The TIQ was below the borderline in six patients.

As shown in Table 7, $CMRO_2$ and TIQ negatively correlated at the significance level of 5% in the left Brodmann areas (BAs) 44,47 and the right BAs 44, 45, 46, and 47. When the p-values were corrected for the B–H procedure, a significant negative correlation between $CMRO_2$ and TIQ was observed in the right BAs 44 and 45 (Table 7 and Figure 15).

Table 7. Pearson's correlation coefficients(r) between TIQ and regional $CMRO_2$

	total IQ		
region	r	p-value	q-value
Lt BA 9	-0.4301	0.1628	0.2035
Lt BA44	-0.5884	*0.0442	0.0884
Lt BA45	-0.2181	0.4959	0.551
Lt BA46	0.0143	0.9647	0.9647
Lt BA47	-0.5826	*0.0468	0.078
Rt BA 9	-0.5557	0.06	0.0857
Rt BA44	-0.7232	*0.0079	**0.0395
Rt BA45	-0.756	*0.0044	**0.044
Rt BA46	-0.6385	*0.0254	0.0635
Rt BA47	-0.6687	*0.0174	0.058

* Demonstrated significant correlation without the Benjamini-Hochberg correction. ($p < 0.05$)

**Demonstrated significant correlation with the Benjamini-Hochberg correction controlled the false discovery rate. ($q < 0.05$)

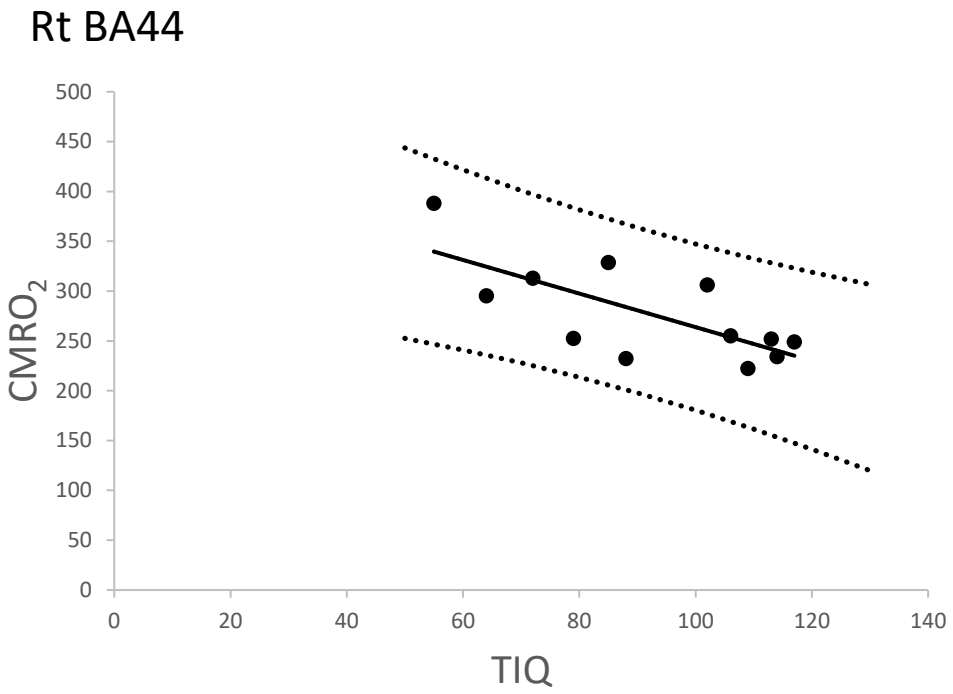

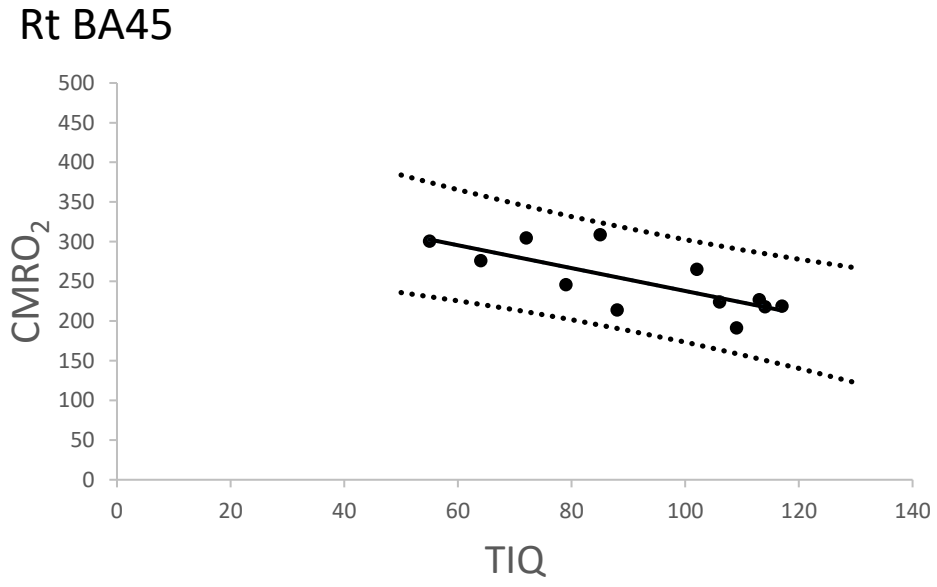

Figure 15. A significant negative correlation between $CMRO_2$ and TIQ was observed in the right BAs 44 and 45.

Discussion

In the patients with neurobehavioral disability following TBI, the $CMRO_2$ in the right BAs 44 and 45 in the resting state significantly increased with decreasing TIQ.

Reports on hypometabolism and hypermetabolism for TBI

There have been numerous reports on regional cerebral metabolism in patients with cognitive function decline following TBI. The rate of regional glycometabolism in TBI patients was lower than that in healthy subjects in some studies [44-48,57]. However, the rate of regional cerebral metabolism in patients with TBI was the same as that in healthy subjects or the rate of regional cerebral metabolism in patients with TBI was higher than that in healthy subjects during task performance in other reports [42 43] . Also, the rate of regional cerebral metabolism partly increased and partly decreased during task performance in another report [58]. As mentioned above, the relationship between cognitive function decline and regional cerebral metabolism has not yet been clarified. To date, there have been many reports that the rate of regional cerebral metabolism in patients with TBI in the resting state was lower than that in the control group and that this hypometabolism was related to functional decline. We also reported that a regional decrease in $CMRO_2$ occurs in some areas in TBI patients without MRI abnormal findings and that these areas seemed to show functional hypometabolism [12].

In this study, however, an increased $CMRO_2$ in the right BAs 44 and 45 was observed in the patients with low IQ. There have been no study in which $CMRO_2$ was assessed to examine the relationship between $CMRO_2$ and IQ in patients with neurobehavioral disability following TBI; this is the first study of such kind. It was considered that the negative correlation between IQ and $CMRO_2$ is related to the plasticity of the brain after TBI.

Plasticity and changes in networks

Significant changes in the nervous system during the long-term functional recovery after TBI are observed in network-level plasticity. The plasticity includes (a) the restructuring of existing networks, (b) the formation of new networks that do not exist under normal conditions, (c) and the restructuring in the undamaged area surrounding the damaged area [59 60].

Although plasticity has beneficial effects by compensatory effects, plasticity can result in harmful changes in the brain in some situations. It has been reported that plasticity induces inappropriate connections between neurons in animals with TBI [61], that epilepsy may be induced by networks changes in TBI models [62].

Because the patients targeted in this study were in the chronic phase, it was possible that plasticity had taken place over a long period after TBI and that the undamaged area of the network consumed an increased amount of energy in order to compensate for the functional decline in the damaged area, as described above (a). Some areas of the human brain are actively working even in the resting state [63]. The resting and active states cannot be clearly distinguished in the human brain. Therefore, our results were consistent with the past reports that the regional cerebral metabolism in TBI patients was higher than the regional cerebral metabolism in the control group in some areas during task performance [42,43 58]. It was considered that the areas of functional decline required an increased amount of energy to remain just as they were during task performance even in the resting state.

The changes in brain networks such as those mentioned above (b) could also be the reason. The studies of patients with TBI using task-based functional magnetic resonance imaging (fMRI) showed that functional networks were damaged and abnormal networks were formed or that new networks were formed to compensate for the functional decline [64-69].

Default mode network (DMN) is the most commonly studied functional network in the resting state. DMN maintains core activity in the resting state [70].

It was reported that the networks in the resting state were also damaged in patients with TBI and that this damage resulted in the changes in the strength of connectivity within DMN or the changes in connectivity between DMN and other networks [71-75]. The results in our study suggest that the changes in the networks in the resting state led to the increased consumption of energy.

One possibility is that regional cerebral metabolism was enhanced to compensate for the functional decline. The other possibility is that new connectivities have pathological effects causing functional decline, which is manifested by a decrease in IQ.

Overview and previous studies of right BAs 44 and 45

Different from other brain areas, BAs 44 and 45 are highly lateralized. The left BAs 44 and 45 are also known as Broca's area, which plays a central role in language function. Broca's area is also involved in working memory, the action perception, the processing of complex inputs [76], and the local visual searching [77 78]. It was also reported that BAs 44 and 45 are bilaterally involved in the encoding of working memory and episodic memory and the selection of motor responses to stimuli [79-81 82]. Although a number of studies have been conducted on Broca's area, there have been fewer studies on the right BAs 44 and 45 and little has been known

about their unique functions. It was reported that the right BAs 44 and 45 are related to the early stage of language learning and acquisition and that the activity shifts to the left side as language acquisition proceeds [83]. Moreover, the right BAs 44 and 45 are involved in the prosodic processing [84 85]. In addition, Sun reported that the right BAs 44 and 45 were related to working memory and short-term memory during the performance of backward and forward digit recall tasks [86]. Kringer–Pedwood reported that the left BA 44 showed greater responses to words than to pictures and that the right BA 44 showed greater responses to pictures than to words [87].

From a morphological perspective, it was previously reported that Broca's area is larger than the contralateral area [88 89]. However, according to a more recent review of many studies including those using modern methods of assessment such as MRI, there is no clear evidence that the left BAs 44 and 45 are more developed than the right BAs 44 and 45 [77]. The right BAs 44 and 45 as well as the left BAs 44 and 45 seem to play a significant role in cognitive function, although the mechanism in the right BAs 44 and 45 is slightly different from that in the left. The results in this study indicate that the increased $CMRO_2$ in the right BAs 44 and 45 compensated for the decline of complicated cognitive function, which is not language-specific.

Limitations

The number of subjects was small in this study. Also, because this study focused on TIQ and the prefrontal area, further research on other functions in other areas is required. In addition, the relationship between the changes in $CMRO_2$ and brain functions during task performance was not clarified because no task was performed in this study. Moreover, the effects of plasticity overtime were unclear because temporal changes were not monitored in this study.

Summary and Conclusion

1. IMZ SPECT is as useful as FMZ PET for evaluating the loss of neuronal integrity in patients presenting with neurobehavioral disability after a TBI.
2. The lower the patient's IQ, the higher the $CMRO_2$ in some areas of prefrontal cortex.

It is preferable to use IMZ SPECT instead of FMZ PET to detect the loss of neuronal integrity, because IMZ SPECT is superior to FMZ PET in terms of versatility. The detection of the loss of neuronal integrity using IMZ SPECT enables the evaluation of the distribution of lesions that cannot be observed by MRI. IMZ SPECT will contribute to the understanding of the cause of neurobehavioral disability in patients with head injuries but showing no abnormalities on MRI images. The clinical symptoms can be better understood when the site of lesions is identified, leading to improved insights into the disease and a better understanding of affected patients among their families and others. In addition, although at this time the treatment of neurobehavioral disabilities involves mainly supportive care (such as the development of compensatory approaches through rehabilitation), the identification of the sites of lesions will help lead to curative treatments with the development of regenerative medicine.

For a thorough understanding of a TBI patient's pathological condition, it is necessary to evaluate not only anatomical lesions but also functional changes.

Investigating the oxygen metabolism changes is considered useful as part of the evaluation of functional changes. Many studies have indicated that hypometabolism is related to functional decline in TBI patients. In clinical settings, hypometabolism and areas of hypoperfusion are often regarded as reflecting functional decline.

In some areas of the prefrontal cortex of TBI patients, the lower the level of cognitive function, the higher the metabolism. In resting cerebral metabolism, it is not only the hypometabolism area that reflects functional deterioration. It is possible that increased metabolism due to brain network changes are related to harmful changes or compensates for functional decline. These findings are considered to develop into a study of the relationship between the resting-state network shown by resting-state functional MRI and brain metabolism shown by molecular imaging.

Acknowledgement

Firstly, I would like to express my gratitude to Professor Katsunori Ikom, the head of department of rehabilitation medicine, Hokkaido university graduate school of medicine, and Professor Nagara Tamaki, the head of department of nuclear medicine, Hokkaido university graduate school of medicine, for giving me the opportunity of this study, and for their thoughtful comments on my research.

Secondly, I really appreciation to Associate Professor Tohru Shiga for mentorship. He supported me strongly from the beginning to the end of my research. Without his guidance, this research would not have possible.

Thirdly, I would like to express my gratitude to Professor Chietsugu Katoh, Faculty of Health Sciences, Hokkaido university graduate school of medicine. He gave great help with the image analysis.

Finally, I would like to offer my special thanks to Dr. Kenji Hirata, Dr. Osamu Manabe, Dr. Kentaro Kobayashi, and Associate Professor Satoshi Ikeda. They provided me valuable comments for statistics and discussion on my research. I would like to also thank to all my colleagues and staff in the Hokkaido university hospital for their supports.

References

1 高村, 政., 丸林, 徹., 三原, 洋., 新田, 雅., 小林, 修., 植村, 正., 矢野, 辰., 大久保, 勝., 中山, 俊., 曽山, 直., 三浦, 正., 三股, 力., 吉田, 顕., 大塚, 忠., 北野, 郁., 藤岡, 正., 不破, 功., 山口, 俊., 恒成, 茂. & 生塩, 之. 熊本県頭部外傷データバンク　これ迄の成果とこれからの課題. *神経外傷* **21**, 118-124 (1998).

2 Alexander, M. P. Mild traumatic brain injury: pathophysiology, natural history, and clinical management. *Neurology* **45**, 1253-1260 (1995).

3 Prevention., C. f. D. C. a. Report to Congress. Traumatic brain injury in the United States: epidemiology and rehabilitation. . (National Center for Injury Prevention and Control; Division of Unintentional Injury Prevention, Atlanta, GA, 2015).

4 Sander, A., Kreutzer, J., Rosenthal, M., Delmonico, R. & Young, M. A Multicenter Longitudinal Investigation of Return to Work and Community Integration Following Traumatic Brain Injury. *The journal of head trauma rehabilitation* **11**, 70-84 (1996).

5 Belanger, H. G., Curtiss, G., Demery, J. A., Lebowitz, B. K. & Vanderploeg, R. D. Factors moderating neuropsychological outcomes following mild traumatic brain injury: a meta-analysis. *J. Int. Neuropsychol. Soc.* **11**, 215-227 (2005).

6 Vanderploeg, R. D., Curtiss, G. & Belanger, H. G. Long-term neuropsychological outcomes following mild traumatic brain injury. *J. Int. Neuropsychol. Soc.* **11**, 228-236 (2005).

7 渡邉, 修., 山口, 武., 橋本, 圭., 猪口, 雄. & 菅原, 誠. 東京都における高次脳機能障害者総数の推計. *The Japanese Journal of Rehabilitation Medicine* **46**, 118-125 (2009).

8 Heiss, W. D., Kracht, L., Grond, M., Rudolf, J., Bauer, B., Wienhard, K. & Pawlik, G. Early [(11)C]Flumazenil/H(2)O positron emission tomography predicts irreversible ischemic cortical damage in stroke patients receiving acute thrombolytic therapy. *Stroke* **31**, 366-369 (2000).

9 Kuroda, S., Shiga, T., Ishikawa, T., Houkin, K., Narita, T., Katoh, C., Tamaki, N. & Iwasaki, Y. Reduced blood flow and preserved vasoreactivity characterize oxygen hypometabolism due to incomplete infarction in occlusive carotid artery diseases. *J. Nucl. Med.* **45**, 943-949 (2004).

10 Sata, Y., Matsuda, K., Mihara, T., Aihara, M., Yagi, K. & Yonekura, Y. Quantitative analysis of benzodiazepine receptor in temporal lobe epilepsy: [(125)I]iomazenil autoradiographic study of surgically resected specimens. *Epilepsia* **43**, 1039-1048 (2002).

11 Morimoto, K., Tamagami, H. & Matsuda, K. Central-type benzodiazepine receptors and epileptogenesis: basic mechanisms and clinical validity. *Epilepsia* **46 Suppl 5**, 184-188 (2005).

12 Shiga, T., Ikoma, K., Katoh, C., Isoyama, H., Matsuyama, T., Kuge, Y., Kageyama, H., Kohno, T., Terae, S. & Tamaki, N. Loss of neuronal integrity: a cause of hypometabolism in patients with traumatic brain injury without MRI abnormality in the chronic stage. *Eur. J. Nucl. Med. Mol. Imaging* **33**, 817-822 (2006).

13 Kawai, N., Maeda, Y., Kudomi, N., Yamamoto, Y., Nishiyama, Y. & Tamiya, T. Focal neuronal damage in patients with neuropsychological impairment after diffuse traumatic brain injury: evaluation using (1)(1)C-flumazenil positron emission tomography with statistical image analysis. *J. Neurotrauma* **27**, 2131-2138 (2010).

14 Lammertsma, A. A. & Hume, S. P. Simplified reference tissue model for PET receptor studies. *Neuroimage* **4**, 153-158 (1996).

15 Millet, P., Graf, C., Buck, A., Walder, B., Westera, G., Broggini, C., Arigoni, M., Slosman, D., Bouras, C. & Ibanez, V. Similarity and robustness of PET and SPECT binding parameters for benzodiazepine receptors. *J. Cereb. Blood Flow Metab.* **20**, 1587-1603 (2000).

16 Shiga, T., Morita, K., Takano, A., Katoh, C., Nakamura, F., Tsukamoto, E., Koyama, T., Iida, H. & Tamaki, N. Clinical advantages of interictal SPECT coregistered to magnetic resonance imaging in patients with epilepsy. *Clin. Nucl. Med.* **26**, 334-339 (2001).

17 Innis, R. B., Cunningham, V. J., Delforge, J., Fujita, M., Gjedde, A., Gunn, R. N., Holden, J., Houle, S., Huang, S. C., Ichise, M., Iida, H., Ito, H., Kimura, Y., Koeppe, R. A., Knudsen, G. M., Knuuti, J., Lammertsma, A. A., Laruelle, M., Logan, J., Maguire, R. P., Mintun, M. A., Morris, E. D., Parsey, R., Price, J. C., Slifstein, M., Sossi, V., Suhara, T., Votaw, J. R., Wong, D. F. & Carson, R. E. Consensus nomenclature for in vivo imaging of reversibly binding radioligands. *J. Cereb. Blood Flow Metab.* **27**, 1533-1539 (2007).

18 Hosokawa, C., Ishii, K., Kimura, Y., Hyodo, T., Hosono, M., Sakaguchi, K., Usami, K., Shimamoto, K., Yamazoe, Y. & Murakami, T. Performance of 11C-Pittsburgh Compound B PET Binding Potential Images in the Detection of Amyloid Deposits on Equivocal Static Images. *J. Nucl. Med.* **56**, 1910-1915 (2015).

19 Logan, J., Fowler, J. S., Volkow, N. D., Wang, G. J., Ding, Y. S. & Alexoff, D. L. Distribution volume ratios without blood sampling from graphical analysis of PET data. *J. Cereb. Blood Flow Metab.* **16**, 834-840 (1996).

20 Wechsler, D. *WAIS-R manual: Wechsler adult intelligence scale-revised*. (Psychological Corporation, 1981).

21 Wechsler, D. Manual for the Wechsler adult intelligence scale-III. *San Antonio, TX: Psychological Corporation* (1997).

22 D, W. Manual for the Wechsler Intelligence Scale for Children-Third Edition. *San Antonio, TX: Psychological Corporation* (1991).

23 Debets, R. M., Sadzot, B., van Isselt, J. W., Brekelmans, G. J., Meiners, L. C., van Huffelen, A. O., Franck, G. & van Veelen, C. W. Is 11C-flumazenil PET superior to 18FDG PET and 123I-iomazenil SPECT in presurgical evaluation of temporal lobe epilepsy? *J. Neurol. Neurosurg. Psychiatry* **62**, 141-150 (1997).

24 Cherry, S. R., Sorenson, J. A. & Phelps, M. E. *Physics in nuclear medicine*. (Elsevier Health Sciences, 2012).

25 Holthoff, V. A., Koeppe, R. A., Frey, K. A., Paradise, A. H. & Kuhl, D. E. Differentiation of

radioligand delivery and binding in the brain: validation of a two-compartment model for [11C]flumazenil. *J. Cereb. Blood Flow Metab.* **11**, 745-752 (1991).

26 Persson, A., Ehrin, E., Eriksson, L., Farde, L., Hedstrom, C. G., Litton, J. E., Mindus, P. & Sedvall, G. Imaging of [11C]-labelled Ro 15-1788 binding to benzodiazepine receptors in the human brain by positron emission tomography. *J. Psychiatr. Res.* **19**, 609-622 (1985).

27 Samson, Y., Hantraye, P., Baron, J. C., Soussaline, F., Comar, D. & Maziere, M. Kinetics and displacement of [11C]RO 15-1788, a benzodiazepine antagonist, studied in human brain in vivo by positron tomography. *Eur. J. Pharmacol.* **110**, 247-251 (1985).

28 Savic, I., Persson, A., Roland, P., Pauli, S., Sedvall, G. & Widen, L. In-vivo demonstration of reduced benzodiazepine receptor binding in human epileptic foci. *Lancet* **2**, 863-866 (1988).

29 Beer, H. F., Blauenstein, P. A., Hasler, P. H., Delaloye, B., Riccabona, G., Bangerl, I., Hunkeler, W., Bonetti, E. P., Pieri, L., Richards, J. G. & et al. In vitro and in vivo evaluation of iodine-123-Ro 16-0154: a new imaging agent for SPECT investigations of benzodiazepine receptors. *J. Nucl. Med.* **31**, 1007-1014 (1990).

30 Johnson, E. W., Woods, S. W., Zoghbi, S., McBride, B. J., Baldwin, R. M. & Innis, R. B. Receptor binding characterization of the benzodiazepine radioligand 125I-Ro16-0154: potential probe for SPECT brain imaging. *Life Sci.* **47**, 1535-1546 (1990).

31 Gentry, L. R., Godersky, J. C. & Thompson, B. MR imaging of head trauma: review of the distribution and radiopathologic features of traumatic lesions. *AJR Am. J. Roentgenol.* **150**, 663-672 (1988).

32 Adams, J. H., Graham, D. I., Murray, L. S. & Scott, G. Diffuse axonal injury due to nonmissile head injury in humans: an analysis of 45 cases. *Ann. Neurol.* **12**, 557-563 (1982).

33 Adams, J. H., Doyle, D., Graham, D. I., Lawrence, A. E. & McLellan, D. R. Gliding contusions in nonmissile head injury in humans. *Arch. Pathol. Lab. Med.* **110**, 485-488 (1986).

34 Kelley, B. J., Farkas, O., Lifshitz, J. & Povlishock, J. T. Traumatic axonal injury in the perisomatic domain triggers ultrarapid secondary axotomy and Wallerian degeneration. *Exp. Neurol.* **198**, 350-360 (2006).

35 Raghupathi, R., Conti, A. C., Graham, D. I., Krajewski, S., Reed, J. C., Grady, M. S., Trojanowski, J. Q. & McIntosh, T. K. Mild traumatic brain injury induces apoptotic cell death in the cortex that is preceded by decreases in cellular Bcl-2 immunoreactivity. *Neuroscience* **110**, 605-616 (2002).

36 Iida, H., Narita, Y., Kado, H., Kashikura, A., Sugawara, S., Shoji, Y., Kinoshita, T., Ogawa, T. & Eberl, S. Effects of scatter and attenuation correction on quantitative assessment of regional cerebral blood flow with SPECT. *J. Nucl. Med.* **39**, 181-189 (1998).

37 Meikle, S. R., Hutton, B. F. & Bailey, D. L. A transmission-dependent method for scatter correction in SPECT. *J. Nucl. Med.* **35**, 360-367 (1994).

38 Axelsson, B., Msaki, P. & Israelsson, A. Subtraction of Compton-scattered photons in single-photon emission computerized tomography. *J. Nucl. Med.* **25**, 490-494 (1984).

39 Ichise, M., Chung, D. G., Wang, P., Wortzman, G., Gray, B. G. & Franks, W. Technetium-99m-HMPAO SPECT, CT and MRI in the evaluation of patients with chronic traumatic brain injury: a correlation with neuropsychological performance. *J. Nucl. Med.* **35**, 217-226 (1994).

40 Goshen, E., Zwas, S. T., Shahar, E. & Tadmor, R. The role of 99Tcm-HMPAO brain SPET in paediatric traumatic brain injury. *Nucl. Med. Commun.* **17**, 418-422 (1996).

41 Millet, P., Graf, C., Buck, A., Walder, B. & Ibanez, V. Evaluation of the reference tissue models for PET and SPECT benzodiazepine binding parameters. *Neuroimage* **17**, 928-942 (2002).

42 Humayun, M. S., Presty, S. K., Lafrance, N. D., Holcomb, H. H., Loats, H., Long, D. M., Wagner, H. N. & Gordon, B. Local cerebral glucose abnormalities in mild closed head injured patients with cognitive impairments. *Nucl. Med. Commun.* **10**, 335-344 (1989).

43 Gross, H., Kling, A., Henry, G., Herndon, C. & Lavretsky, H. Local cerebral glucose metabolism in patients with long-term behavioral and cognitive deficits following mild traumatic brain injury. *J. Neuropsychiatry Clin. Neurosci.* **8**, 324-334 (1996).

44 Ruff, R. M., Crouch, J. A., Troster, A. I., Marshall, L. F., Buchsbaum, M. S., Lottenberg, S. & Somers, L. M. Selected cases of poor outcome following a minor brain trauma: comparing neuropsychological and positron emission tomography assessment. *Brain Inj.* **8**, 297-308 (1994).

45 Umile, E. M., Sandel, M. E., Alavi, A., Terry, C. M. & Plotkin, R. C. Dynamic imaging in mild traumatic brain injury: support for the theory of medial temporal vulnerability. *Arch. Phys. Med. Rehabil.* **83**, 1506-1513 (2002).

46 Kato, T., Nakayama, N., Yasokawa, Y., Okumura, A., Shinoda, J. & Iwama, T. Statistical image analysis of cerebral glucose metabolism in patients with cognitive impairment following diffuse traumatic brain injury. *J. Neurotrauma* **24**, 919-926 (2007).

47 Provenzano, F. A., Jordan, B., Tikofsky, R. S., Saxena, C., Van Heertum, R. L. & Ichise, M. F-18 FDG PET imaging of chronic traumatic brain injury in boxers: a statistical parametric analysis. *Nucl. Med. Commun.* **31**, 952-957 (2010).

48 Peskind, E. R., Petrie, E. C., Cross, D. J., Pagulayan, K., McCraw, K., Hoff, D., Hart, K., Yu, C. E., Raskind, M. A., Cook, D. G. & Minoshima, S. Cerebrocerebellar hypometabolism associated with repetitive blast exposure mild traumatic brain injury in 12 Iraq war Veterans with persistent post-concussive symptoms. *Neuroimage* **54 Suppl 1**, S76-82 (2011).

49 Tanji, J. & Hoshi, E. Role of the lateral prefrontal cortex in executive behavioral control. *Physiol. Rev.* **88**, 37-57 (2008).

50 Duncan, J., Seitz, R. J., Kolodny, J., Bor, D., Herzog, H., Ahmed, A., Newell, F. N. & Emslie, H. A neural basis for general intelligence. *Science* **289**, 457-460 (2000).

51 Gray, J. R., Chabris, C. F. & Braver, T. S. Neural mechanisms of general fluid intelligence. *Nat. Neurosci.* **6**, 316-322 (2003).

52 van Veluw, S. J., Sawyer, E. K., Clover, L., Cousijn, H., De Jager, C., Esiri, M. M. & Chance, S. A. Prefrontal cortex cytoarchitecture in normal aging and Alzheimer's disease: a relationship with IQ. *Brain structure & function* **217**, 797-808 (2012).

53 Skranes, J., Lohaugen, G. C., Martinussen, M., Haberg, A., Brubakk, A. M. & Dale, A. M. Cortical surface area and IQ in very-low-birth-weight (VLBW) young adults. *Cortex* **49**, 2264-2271 (2013).

54 Larrabee, G. J. Another look at VIQ-PIQ scores and unilateral brain damage. *Int. J. Neurosci.* **29**, 141-148 (1986).

55 Iverson, G. L., Mendrek, A. & Adams, R. L. The persistent belief that VIQ-PIQ splits suggest lateralized brain damage. *Appl. Neuropsychol.* **11**, 85-90 (2004).

56 Matarazzo, J. D. & Herman, D. O. Base rate data for the WAIS-R: test-retest stability and VIQ-PIQ differences. *J. Clin. Neuropsychol.* **6**, 351-366 (1984).

57 Nakayama, N., Okumura, A., Shinoda, J., Nakashima, T. & Iwama, T. Relationship between regional cerebral metabolism and consciousness disturbance in traumatic diffuse brain injury without large focal lesions: an FDG-PET study with statistical parametric mapping analysis. *J. Neurol. Neurosurg. Psychiatry* **77**, 856-862 (2006).

58 Zhang, J., Mitsis, E. M., Chu, K., Newmark, R. E., Hazlett, E. A. & Buchsbaum, M. S. Statistical parametric mapping and cluster counting analysis of [18F] FDG-PET imaging in traumatic brain injury. *J. Neurotrauma* **27**, 35-49 (2010).

59 Munoz-Cespedes, J. M., Rios-Lago, M., Paul, N. & Maestu, F. Functional neuroimaging studies of cognitive recovery after acquired brain damage in adults. *Neuropsychol. Rev.* **15**, 169-183 (2005).

60 Berlucchi, G. Brain plasticity and cognitive neurorehabilitation. *Neuropsychol. Rehabil.* **21**, 560-578 (2011).

61 Li, N., Yang, Y., Glover, D. P., Zhang, J., Saraswati, M., Robertson, C. & Pelled, G. Evidence for impaired plasticity after traumatic brain injury in the developing brain. *J. Neurotrauma* **31**, 395-403 (2014).

62 Hunt, R. F., Scheff, S. W. & Smith, B. N. Posttraumatic epilepsy after controlled cortical impact injury in mice. *Exp. Neurol.* **215**, 243-252 (2009).

63 Raichle, M. E., MacLeod, A. M., Snyder, A. Z., Powers, W. J., Gusnard, D. A. & Shulman, G. L. A default mode of brain function. *Proc. Natl. Acad. Sci. U. S. A.* **98**, 676-682 (2001).

64 McAllister, T. W., Saykin, A. J., Flashman, L. A., Sparling, M. B., Johnson, S. C., Guerin, S. J., Mamourian, A. C., Weaver, J. B. & Yanofsky, N. Brain activation during working memory 1 month after mild traumatic brain injury: a functional MRI study. *Neurology* **53**, 1300-1308 (1999).

65 Perlstein, W. M., Cole, M. A., Demery, J. A., Seignourel, P. J., Dixit, N. K., Larson, M. J. &

Briggs, R. W. Parametric manipulation of working memory load in traumatic brain injury: behavioral and neural correlates. *J. Int. Neuropsychol. Soc.* **10**, 724-741 (2004).

66 Rasmussen, I. A., Xu, J., Antonsen, I. K., Brunner, J., Skandsen, T., Axelson, D. E., Berntsen, E. M., Lydersen, S. & Haberg, A. Simple dual tasking recruits prefrontal cortices in chronic severe traumatic brain injury patients, but not in controls. *J. Neurotrauma* **25**, 1057-1070 (2008).

67 Turner, G. R. & Levine, B. Augmented neural activity during executive control processing following diffuse axonal injury. *Neurology* **71**, 812-818 (2008).

68 Kim, Y. H., Yoo, W. K., Ko, M. H., Park, C. H., Kim, S. T. & Na, D. L. Plasticity of the attentional network after brain injury and cognitive rehabilitation. *Neurorehabil. Neural Repair* **23**, 468-477 (2009).

69 Kasahara, M., Menon, D. K., Salmond, C. H., Outtrim, J. G., Tavares, J. V., Carpenter, T. A., Pickard, J. D., Sahakian, B. J. & Stamatakis, E. A. Traumatic brain injury alters the functional brain network mediating working memory. *Brain Inj.* **25**, 1170-1187 (2011).

70 Buckner, R. L. & Vincent, J. L. Unrest at rest: default activity and spontaneous network correlations. *Neuroimage* **37**, 1091-1096; discussion 1097-1099 (2007).

71 Sharp, D. J., Beckmann, C. F., Greenwood, R., Kinnunen, K. M., Bonnelle, V., De Boissezon, X., Powell, J. H., Counsell, S. J., Patel, M. C. & Leech, R. Default mode network functional and structural connectivity after traumatic brain injury. *Brain* **134**, 2233-2247 (2011).

72 Mayer, A. R., Mannell, M. V., Ling, J., Gasparovic, C. & Yeo, R. A. Functional connectivity in mild traumatic brain injury. *Hum. Brain Mapp.* **32**, 1825-1835 (2011).

73 Zhou, Y., Milham, M. P., Lui, Y. W., Miles, L., Reaume, J., Sodickson, D. K., Grossman, R. I. & Ge, Y. Default-mode network disruption in mild traumatic brain injury. *Radiology* **265**, 882-892 (2012).

74 Sours, C., Zhuo, J., Janowich, J., Aarabi, B., Shanmuganathan, K. & Gullapalli, R. P. Default mode network interference in mild traumatic brain injury - a pilot resting state study. *Brain Res.* **1537**, 201-215 (2013).

75 Venkatesan, U. M., Dennis, N. A. & Hillary, F. G. Chronology and chronicity of altered resting-state functional connectivity after traumatic brain injury. *J. Neurotrauma* **32**, 252-264 (2015).

76 Grodzinsky, Y. & Santi, A. The battle for Broca's region. *Trends in cognitive sciences* **12**, 474-480 (2008).

77 Keller, S. S., Crow, T., Foundas, A., Amunts, K. & Roberts, N. Broca's area: nomenclature, anatomy, typology and asymmetry. *Brain Lang.* **109**, 29-48 (2009).

78 Fink, G. R., Manjaly, Z. M., Stephan, K. E., Gurd, J. M., Zilles, K., Amunts, K. & Marshall, J. C. *A role for Broca's area beyond language processing: evidence from neuropsychology and fMRI.* (New York: Oxford University Press, 2006).

79 Ranganath, C., Johnson, M. K. & D'Esposito, M. Prefrontal activity associated with working

memory and episodic long-term memory. *Neuropsychologia* **41**, 378-389 (2003).

80 Fletcher, P. C. & Henson, R. N. Frontal lobes and human memory: insights from functional neuroimaging. *Brain* **124**, 849-881 (2001).

81 Koechlin, E., Ody, C. & Kouneiher, F. The architecture of cognitive control in the human prefrontal cortex. *Science* **302**, 1181-1185 (2003).

82 Minamoto, T., Yaoi, K., Osaka, M. & Osaka, N. The rostral prefrontal cortex underlies individual differences in working memory capacity: An approach from the hierarchical model of the cognitive control. *Cortex* **71**, 277-290 (2015).

83 Sugiura, L., Ojima, S., Matsuba-Kurita, H., Dan, I., Tsuzuki, D., Katura, T. & Hagiwara, H. Sound to language: different cortical processing for first and second languages in elementary school children as revealed by a large-scale study using fNIRS. *Cereb. Cortex* **21**, 2374-2393 (2011).

84 Pugh, K. R., offywitz, B. A., Shaywitz, S. E., Fulbright, R. K., Byrd, D., Skudlarski, P., Shankweiler, D. P., Katz, L., Constable, R. T., Fletcher, J., Lacadie, C., Marchione, K. & Gore, J. C. Auditory selective attention: an fMRI investigation. *Neuroimage* **4**, 159-173 (1996).

85 Celsis, P., Boulanouar, K., Doyon, B., Ranjeva, J. P., Berry, I., Nespoulous, J. L. & Chollet, F. Differential fMRI responses in the left posterior superior temporal gyrus and left supramarginal gyrus to habituation and change detection in syllables and tones. *Neuroimage* **9**, 135-144 (1999).

86 Sun, X., Zhang, X., Chen, X., Zhang, P., Bao, M., Zhang, D., Chen, J., He, S. & Hu, X. Age-dependent brain activation during forward and backward digit recall revealed by fMRI. *Neuroimage* **26**, 36-47 (2005).

87 Krieger-Redwood, K., Teige, C., Davey, J., Hymers, M. & Jefferies, E. Conceptual control across modalities: graded specialisation for pictures and words in inferior frontal and posterior temporal cortex. *Neuropsychologia* **76**, 92-107 (2015).

88 Falzi, G., Perrone, P. & Vignolo, L. A. Right-left asymmetry in anterior speech region. *Arch. Neurol.* **39**, 239-240 (1982).

89 Amunts, K., Schleicher, A., Burgel, U., Mohlberg, H., Uylings, H. B. & Zilles, K. Broca's region revisited: cytoarchitecture and intersubject variability. *J Comp Neurol.* **412**, 319-341. (1999).